Hindawi
International Journal of Aerospace Engineering
Volume 2021, Article ID 8880387, 12 pages
https://doi.org/10.1155/2021/8880387

Research Article

Prescribed Performance Tracking Control for the Hypersonic Vehicle with Actuator Faults

Zhenghui Yang,[1] Wentao He,[2] Yushan He,[3] Yaen Xie,[2] Jun Li,[3] and Shuo Song[3]

[1]*School of Geological Engineering and Geomatics, Chang'an University, China*
[2]*College of Aerospace and Civil Engineering, Harbin Engineering University, China*
[3]*School of Automation, Harbin Engineering University, China*

Correspondence should be addressed to Yaen Xie; xieenya@126.com

Received 19 September 2020; Revised 22 February 2021; Accepted 10 March 2021; Published 31 March 2021

Academic Editor: Maj D. Mirmirani

This paper provides a solution for the trajectory tracking control of a hypersonic flight vehicle (HFV), which is encountered performance constraints, actuator faults, external disturbances, and system uncertainties. For the altitude and velocity control subsystems, the backstepping-based dynamic surface control (DSC) strategy is constructed to guarantee the predefined constraint of tracking errors. The introduction of first-order low-pass filters effectively remedies the problem of "complexity explosion" existing in high-order backstepping design. Simultaneously, radial basis function neural networks (RBFNNs) are adopted for approximating the unavailable dynamics, in which the minimum learning parameter (MLP) algorithm brilliantly alleviates the excessive occupation of the computational resource. Specially, in consideration of the unknown actuator failures, the adaptive signals are designed to enhance the reliability of the closed-loop system. Finally, according to rigorous theoretical analysis and simulation experiment, the stability of the proposed controller is verified, and its superiority is exhibited intuitively.

1. Introduction

The recent few years have witnessed the burgeoning interest in hypersonic flight vehicles (HFVs) from researchers owing to its unique advantages like rapid maneuver and high efficiency. In light of these inherent characteristics, HFVs have been extensively applied in both military and civilian fields. However, there are still many obstructions in constructing controllers for HFVs, involving the harsh flight environment, the uncertainty of aerodynamics, and the strong nonlinearity and coupling. In order to surmount these challenges, numerous control frameworks have been examined, just to name a few, sliding mode control (SMC) [1–4], backstepping control [5–8], dynamic surface control (DSC) [9, 10], adaptive control [11, 12], and so forth.

As a classical nonlinear control approach, SMC is celebrated for its antidisturbance capability, easy implementation, and excellent robustness [13–16]. In [1], SMC-based architecture was established to achieve the trajectory tracking control for HFV, while it comes with the undesired phenomenon of chattering. This defect will undoubtedly generate a heavy burden on actuators and shorten their service lives. Fortunately, [2] provided a continuous antichattering sliding mode controller for the flexible HFVs. Besides the SMC methods, the backstepping-based procedure design possesses a high application value in high-order nonlinear systems. The disadvantage of traditional backstepping methods lies in the issue of "complexity explosion," which always leads to waste of computational resources and excessive hardware requirements. Therefore, the DSC-based solution was developed in [9] so that the above problem could be relaxed by resorting to the introduction of low-pass filters. In addition, complicated aerodynamics is another threat for trajectory tracking of HFVs. Inaccurate dynamics makes model-dependent control schemes uncapable for practical engineering. Inspired by this condition, a neural adaptive sliding mode control algorithm was proposed in [17], where the radial basis function neural networks (RBFNNs) were utilized to approximate the available dynamics with an exacting precision.

At the same time, while accounting for the uncertainties of HFV models, great demands were placed on the convergence rate and tracking accuracy of control systems [18]. From this view of point, most of the aforementioned controllers possess satisfactory steady-state characteristics but lack specific constraints on transient performances. Under this urgent requirement, the prescribed performance control (PPC) technology is introduced to restrict certain states within a predefined region globally [19–24], such that the system transient indicators can be flexibly specified by the designers. Therefore, Shao et al. imposed time performance constraints in event-triggered robust control for quadrotors, which apparently optimized the stable rate of the closed-loop system [19]. As for the PPC strategy in vehicle control field, Bu constructed a RBFNN-based robust algorithm for air-breathing hypersonic vehicles (AHVs) with unknown dead-zone input nonlinearity, where the trajectory tracking errors are effectively suppressed within a predetermined range [21].

However, the controllers mentioned above are all designed on basis of the assumption that actuators of HFVs work normally. Obviously, it is of impractical conceit for HFV servicing in ideal environments. To prevent the resulting performance degradation and instable phenomenon, the actuator faults must be taken into account while formulating the trajectory tracking control strategies with sufficient applicability and reliability [25–27]. In [26], a quasi-continuous high-order sliding mode framework was presented, in which the neural network observer is introduced to ensure the convergence of estimation errors. Further in [28], an adaptive fault-tolerant control scheme was derived in the presence of actuator saturation to improve system reliability and robustness. By the utilization of PPC, a fault-tolerant protocol was designed to achieve the accurate trajectory tracking for HFVs.

Driven by the aforementioned observations, this paper aims at the prescribed performance fault-tolerant control for HFV suffering from system uncertainties and actuator failures. The backstepping-based dynamic surface design is conducted to guarantee the finite-time convergence of altitude and velocity tracking errors. Unknown multiplicative and additive faults of actuators are handled by resorting to the construction of adaptive architectures. On the other hand, unmodeled dynamics are approximated via RBFNNs; especially, the minimum learning parameter (MLP) algorithm requires less computational resource. Finally, the stability and superiority of the proposed controller will be corroborated by theoretical analysis and simulation experiments. It will be elaborated that the transient and steady-state performance constraints are always satisfied. Contributions of this article are presented as follows:

(1) Different from the traditional approximation of RBFNN [12, 17], MLP algorithm is utilized to cope with the uncertain dynamics in this paper. In this way, it is no longer necessary to estimate the entire weight matrix, but the upper bound of its norm is taken as the object of online updating. Therefore, the computational complexity is considerably degraded, and the hardware requirement is reduced significantly

(2) In [23, 24], PPC control methods were presented for MEMS Gyroscopes and Networked Uncertain Quadrotors, respectively, which cannot be directly applied for hypersonic vehicles. Considering this point, the PPC-based dynamic surface controller is synthesized for hypersonic vehicles in the presence of uncertainties, actuator faults, and disturbances. The results of this paper could be treated as an application of PPC for hypersonic vehicles

(3) Instead of restricting the time performance [19, 20], the PPC-based amplitude constraints [23, 24] of HFVs' trajectory tracking errors are addressed in this paper. In virtue of the hyperbolic tangent function, the open-loop tracking error dynamics with certain designer-specified index constraints is transformed into an equivalent "state-constrained" system, in which both transient and steady-state responses obtain the satisfactory performance

The remainder of this paper is organized as follows. Section 2 gives a longitudinal model of HFVs and the relative preliminaries. The altitude and velocity controllers are designed in Section 3 and Section 4, respectively. In Section 5, the validity of the controllers is verified through a simulation experiment. Finally, Section 6 shows the conclusion of this work.

2. Problem Formulation

2.1. Longitudinal Model of HFV. The trajectory tracking control problem for a HFV is considered in this paper. According to [29], the longitudinal model of the HFV can be expressed as:

$$\dot{V} = \frac{T\cos\alpha - D}{m} - \frac{\mu\sin\gamma}{r^2}, \tag{1}$$

$$\dot{\gamma} = \frac{L + T\sin\alpha}{mV} - \frac{\left(\mu - \mathrm{V}^2\mathrm{r}\right)\cos\gamma}{Vr^2}, \tag{2}$$

$$\dot{h} = V\sin\gamma, \tag{3}$$

$$\dot{\alpha} = q - \dot{\gamma}, \tag{4}$$

$$\dot{q} = \frac{M_{yy}}{I_{yy}}. \tag{5}$$

The corresponding dynamics are given as:

$$L = \bar{q}SC_L, \tag{6}$$

$$D = \bar{q}SC_D, \tag{7}$$

$$T = \bar{q}SC_T, \tag{8}$$

$$M_{yy} = \bar{q}S\bar{c}[C_M(\alpha) + C_M(\delta) + C_M(q)], \tag{9}$$

$$r = h + r_e, \tag{10}$$

$$C_L = 0.6203\alpha, \tag{11}$$

$$C_D = 0.6450\alpha^2 + 0.0043378\alpha + 0.003772, \tag{12}$$

$$C_T = \begin{cases} 0.022576\beta & \beta < 1 \\ 0.0224 + 0.00336\beta & \beta > 1 \end{cases}, \tag{13}$$

$$C_M(\alpha) = -0.035\alpha^2 + 0.036117\alpha + 5.3261 \times 10^{-6}, \tag{14}$$

$$C_M(q) = \frac{\bar{c}q\left(-0.6796\alpha^2 + 0.3015\alpha - 0.2289\right)}{2V}, \tag{15}$$

$$C_M(\delta_e) = c_e(\delta_e - \alpha), \tag{16}$$

$$c_e = 0.0292, \tag{17}$$

where $\bar{c}$ and c_e denote constants; $\bar{q}$ denotes the dynamic pressure satisfying $\bar{q} = (1/2)\rho V^2$; V, h, γ, α, and q denote velocity, altitude, flight path angle, angle of attack, and pitch rate of HFV, respectively [30]; T, D, L, and Myy denote the thrust of the engine, drag force, lift force, and pitching moment, respectively [31]; and S, m, ρ, I_{yy}, μ, and r_e denote the reference area, mass, density of air, moment of inertia, the gravitational constant, and radius of the Earth, respectively [32].

As a matter of fact, various unexpected failures occur to the actuators frequently in practical engineering, which will cause severe performance degradation and even collapse for whole close-loop system. Therefore, it is necessary to take the actuator faults into consideration while designing the trajectory tracking controllers. With the introduction of multiplicative and additive faults, the actual input signal is described as:

$$\delta_e = \rho_i u_c + d_i(\mathrm{t}) + \Delta_i, \tag{18}$$

where ρ_i denotes the unknown effectiveness factor of actuator and satisfies $0 < \iota_i \le \rho_i \le 1$, $\iota_i \le 1$ represents the minimum value of ρ_i, $d_i(\mathrm{t})$ denotes the unknown external disturbance, and Δ_i is the additive fault with $i = 1, 2$.

2.2. Fundamental of RBFNNs. RBFNN is an effective tool to obtain the approximation of unknown system dynamics. The following lemma sketches the basic principle of RBFNNs.

$$f(\mathbf{x}) = \mathbf{W}^{*\mathrm{T}}\mathbf{H}(\mathbf{x}) + r, 0 < |r| \le O. \tag{19}$$

Lemma 1 [33]. *An arbitrary continuous smooth function $f(x)$ can be described as the following form by defining a basis function $H(x)$.*

Here, $\mathbf{W}^* = [W_{a1}, W_{a2}, \cdots, W_{ap}]^T$ is the ideal weight matrix, and $\mathbf{x} = [x_{a1}, x_{a2}, \cdots, x_{am}]$ represents the input vector. r and O are the additional approximation error and its upper bound; $\mathbf{H}(\mathbf{x}) = [H_{a1}(\mathbf{x}), H_{a2}(\mathbf{x}), \cdots, H_{am}(\mathbf{x})]^{\mathrm{T}}$ is selected as the Gaussian basis function, which can be expressed as:

$$H_{ai}(\mathbf{x}) = \exp\left(-\frac{\|\mathbf{x} - \mathbf{c_i}\|_2^2}{2b_i^2}\right), i = 1, \cdots, p, \tag{20}$$

with $c_i \in R^m$ and $b \in R^p$ denoting the center vector and the width of Gaussian basis function, respectively.

2.3. Other Preliminaries

Lemma 2 [33]. *For arbitrary scalar $x \in R$ and $\mu > 0$, the inequation about hyperbolic tangent function is shown as:*

$$0 < |x| - x \tanh(\mu x) \le \frac{\kappa}{\mu}, \tag{21}$$

in which the constant $\kappa = 0.2785$.

Assumption 3. The additive actuator fault and external disturbances are both unknown but bounded, which are supposed to satisfy $|d_i(\mathrm{t}) + \Delta_i| \le \lambda_i (i = 1, 2)$ with λ_i being positive constants.

3. Altitude Controller Design

Aiming towards the altitude and velocity tracking missions, two subsystems are formulated on basis of the longitudinal model of HFV. In this section, a DSC-based adaptive fault-tolerant controller is constructed for the altitude tracking subsystem. Due to the high-order characteristic of the dynamics, traditional backstepping design is inevitably accompanied by the phenomenon of "complexity explosion," which is arising from the frequent differential to virtual commands. Therefore, low-pass filters are introduced to solve this problem, while system uncertainties are handled via RBFNN. Finally, it is validated via Lyapunov-based analysis that altitude tracking errors exponentially converge to a tiny region containing the origin.

In altitude tracking control subsystem, three states are selected as γ, ϑ_p, and q. To facilitate the subsequent design, a state vector is defined as:

$$\mathbf{x} = [x_1, x_2, x_3]^T = \left[\gamma, \vartheta_p, q\right]^T, \tag{22}$$

where $\vartheta_p = \alpha + \gamma$. Thus, the altitude dynamics can be described as [30]:

$$\begin{aligned} \dot{x}_1 &= f_1(x_1, V) + \mathrm{g}_1(V)x_2, \\ \dot{x}_2 &= f_2 + g_2 x_3, \\ \dot{x}_3 &= f_3(x_1, x_2, x_3, V) + g_3(V)\delta_e = f_3(x_1, x_2, x_3, V) \\ &\quad + g_3(V)(\rho_1 u_{c1} + d_1(t) + \Delta_1), \end{aligned} \tag{23}$$

with

$$g_1(V) = \frac{0.31015\rho VS}{m},$$
$$f_1(x_1, V) = \frac{T\sin\alpha}{mV} - \frac{\left(\mu\text{-}V^2 r\right)\cos\gamma}{Vr^2},$$
$$f_2 = 0, g_2 = 1,$$
$$f_3(x_1, x_2, x_3, V) = \frac{0.5\rho V^2 S(C_M(\alpha) + C_M(q) - c_e\alpha)}{I_{yy}},$$
$$g_3(V) = \frac{\bar{q}S\bar{c}c_e}{I_{yy}}. \tag{24}$$

Assumption 4. The uncertain term $g_i(V)$ possesses an upper bound $\bar{g}_i$, which satisfies $0 < |g_i(V)| \le \bar{g}_i$, $i = 1, 3$.

At this moment, the control objective has been transformed into forcing $x_i(i = 0, 1, 2, 3)$ to track the desired trajectories, where $x_0 = h$. For this purpose, the tracking error variables are introduced as $x_{ei} = x_i - x_{id}$ with $x_{0d} = h_d$, $x_{1d} = \gamma_d$, $x_{2d} = \vartheta_{pd}$, and $x_{3d} = q_d$ denoting reference states.

To ensure the prescribed performance, the boundary of variable x_{ei} is defined as:

$$\underline{x}_{ei} \le x_{ei} \le \bar{x}_{ei}. \tag{25}$$

The error transformation is designed as:

$$x_{ei} = \frac{\bar{x}_{ei} - \underline{x}_{ei}}{2}\tanh(s_i) + \frac{\bar{x}_{ei} + \underline{x}_{ei}}{2}, \tag{26}$$

$$s_i = \operatorname{atanh}\left(\frac{2x_{ei} - \bar{x}_{ei} - \underline{x}_{ei}}{\bar{x}_{ei} - \underline{x}_{ei}}\right), \tag{27}$$

in which s_i is the transformed tracking error. It indicates that the transformed error increases monotonically with the original variable.

Note additionally that there exist limits as:

$$\lim_{s_i \to -\infty} x_{ei} = \underline{x}_{ei}, \lim_{s_i \to +\infty} x_{ei} = \bar{x}_{ei}. \tag{28}$$

Necessarily, the time derivative of s_i is derived as:

$$\dot{s}_i = m_i \dot{x}_{ei} + n_i, \tag{29}$$

in which $m_i = \partial s_i/\partial x_{ei}$, $n_i = (\partial s_i/\partial \bar{x}_{ei})\dot{\bar{x}}_{ei} + (\partial s_i/\partial x_{-ei})\dot{x}_{-ei}$ with $i = 1, 2, 3$.

Step 1. According to Equation (29), the derivative of s_0 satisfies the following equation:

$$\dot{s}_0 = m_0 \dot{x}_{e0} + n_0 = m_0 V \sin(x_1) + n_0. \tag{30}$$

Based on the similar analysis in [34], the asymptotic stability of the altitude tracking error x_{e0} is ensured if the virtual command is designed as:

$$x_{1d} = \arcsin\left(\frac{-k_h s_0 - k_{hh} s_0 + \dot{h}_d + n_0}{m_0 V}\right), \tag{31}$$

with $k_h > 0$, $k_{hh} > 0$. For the purpose of stabilizing x_{e1}, the following equations are firstly presented by utilizing Equations (24) and (26)–(29):

$$\begin{aligned} \dot{x}_{e1} &= f_1 + g_1 x_2 - \dot{x}_{1d}, \\ \dot{s}_1 &= m_1 \dot{x}_{e1} + n_1 \\ &= m_1(f_1 + g_1 x_2 - \dot{x}_{1d}) + n_1. \end{aligned} \tag{32}$$

A first-order low-pass filter is introduced as:

$$\varepsilon_2 \dot{x}_{2d} + x_{2d} = x_{2c}, x_{2d}(0) = x_{2c}(0), \tag{33}$$

where the variable x_{2c} represents the filtered signal and $\varepsilon_2 > 0$ is a constant.

To cope with the unavailable dynamic $m_1 f_1$, Lemma 1 is applied here. Then, one has:

$$\begin{aligned} m_1 f_1 &= \mathbf{W}_{a1}^{*T}\mathbf{H}_{a1}(\mathbf{x}) + r_1, 0 < |r_1| \le O_1, \\ \left\|\mathbf{W}_{a1}^{*T}\mathbf{H}_{a1}\right\| &\le \left\|\mathbf{W}_{a1}^{*T}\right\|\left\|\mathbf{H}_{a1}\right\| \le w_1 h_1, \end{aligned} \tag{34}$$

where $h_1 = \|\mathbf{H}_{a1}\|$ and $w_1 \ge \|\mathbf{W}_{a1}^{*T}\|$.

By defining that $R_1 = O_1$, the virtual control input and the relevant adaptive laws are designed as:

$$\begin{aligned} x_{2c} = \frac{1}{g_1}\Bigg[&\dot{x}_{1d} - g_1 x_{e2} + \frac{1}{m_1}\left(-\hat{w}_1 h_1 \tanh\left(\frac{s_1}{\mu_1}\right) - \hat{R}_1 \tanh\left(\frac{s_1}{\mu_2}\right)\right. \\ &\left.- k_1 s_1 - k_2 \tanh(s_1) - n_1\right)\Bigg], \end{aligned} \tag{35}$$

$$\dot{\hat{w}}_1 = \alpha_1\left[|s_1| h_1 \tanh\left(\frac{|s_1|}{\mu_1}\right) - c_1 \hat{w}_1\right], \tag{36}$$

$$\dot{\hat{R}}_1 = \beta_1\left[|s_1| \tanh\left(\frac{|s_1|}{\mu_2}\right) - c_2 \hat{R}_1\right], \tag{37}$$

where $\hat{w}_1$ and $\hat{R}_1$ are the estimation values of w_1 and R_1, respectively, and k_1 and k_2 are the positive constants.

Step 2. As for x_2, according to Equations (24) and (26)–(29), one has:

$$\begin{aligned} \dot{x}_{e2} &= \dot{x}_2 - \dot{x}_{2d} = x_3 - \dot{x}_{2d}, \\ \dot{s}_2 &= m_2 \dot{x}_{e2} + n_2 \\ &= m_2(x_3 - \dot{x}_{2d}) + n_2. \end{aligned} \tag{38}$$

A first-order filter is given as:

$$\varepsilon_3 \dot{x}_{3d} + x_{3d} = x_{3c}, x_{3d}(0) = x_{3c}(0), \tag{39}$$

where $\varepsilon_3 > 0$ is a positive constant.

Introduce the virtual command x_{3c}, which is taken as:

$$x_{3c} = \frac{1}{m_2}\left[-k_3 s_2 - k_4 \tanh(s_2) - n_2\right] + \dot{x}_{2d} - x_{e3}, \tag{40}$$

where k_3 and k_4 are the positive constants.

Step 3. To ensure the convergence of x_{e3}, Equations (24) and (26)–(29) are combined, and the following equations are obtained:

$$\dot{x}_{e3} = \dot{x}_3 - \dot{x}_{3d} = f_3 + g_3(\rho_1 u_{c1} + d_1(\mathrm{t}) + \Delta_1) - \dot{x}_{3d}, \tag{41}$$

$$\begin{aligned}\dot{s}_3 &= m_3\dot{x}_{e3} + n_3\\ &= m_3(f_3 + g_3(\rho_1 u_{c1} + d_1(t) + \Delta_1) - \dot{x}_{3d}) + n_3.\end{aligned} \tag{42}$$

By taking the unavailable dynamic $m_3 f_3$ into consideration and according to Lemma 1, one can obtain:

$$m_3 f_3 = \mathbf{W}_{a3}^{*T}\mathbf{H}_{a3}(\mathbf{x}) + r_3, 0 < |r_3| \le O_3, \tag{43}$$

$$\left\|\mathbf{W}_{a3}^{*T}\mathbf{H}_{a3}\right\| \le \left\|\mathbf{W}_{a3}^{*T}\right\|\left\|\mathbf{H}_{a3}\right\| \le w_3 h_3, \tag{44}$$

where $h_3 = \|\mathbf{H}_{a3}\|$ and $w_3 \ge \|\mathbf{W}_{a3}^{*T}\|$.

With the definitions of $R_3 = m_3\bar{g}_3\lambda_1 + O_3$ and $\eta_1 = ((1 - \rho_1)m_3)/\rho_1$, the control input and corresponding adaptive laws are designed as:

$$u_1 = -g_3^{-1}(u_{\text{nom1}} + u_{n1}), \tag{45}$$

$$u_{\text{nom1}} = \frac{1}{m_3}\left[\widehat{w}_3 h_3 \tanh\left(\frac{s_3}{\mu_3}\right) + \widehat{R}_3 \tanh\left(\frac{s_3}{\mu_4}\right) + k_5 s_3 + k_6 \tanh(s_3) + n_3\right] - \dot{x}_{3d}, \tag{46}$$

$$u_{n1} = \frac{1}{m_3}\widehat{\eta}_1|u_{\text{nom1}}| \tanh\left(\frac{|u_{\text{nom1}}|s_3}{\mu_5}\right), \tag{47}$$

$$\dot{\widehat{\eta}}_1 = k_7\left[|u_{\text{nom1}}||s_3| \tanh\left(\frac{|u_{\text{nom1}}||s_3|}{\mu_5}\right) - k_8\widehat{\eta}_1\right], \tag{48}$$

$$\dot{\widehat{w}}_3 = \alpha_3\left[|s_3|h_3 \tanh\left(\frac{|s_3|}{\mu_3}\right) - c_5\widehat{w}_3\right], \tag{49}$$

$$\dot{\widehat{R}}_3 = \beta_3\left[|s_3| \tanh\left(\frac{|s_3|}{\mu_4}\right) - c_6\widehat{R}_3\right], \tag{50}$$

where $\widehat{\eta}_1$, $\widehat{w}_3$, and $\widehat{R}_3$ are estimations of η_1, w_3, and R_3, respectively, and k_5, k_6,k_7, k_8, α_3, β_3, c_5, c_6, μ_3, and μ_4 are all positive constants.

Theorem 5. *For the HFV system (24), if the virtual commands are designed as Equations (31), (35), and (40), control signals are designed as Equations (45)–(47); it can be concluded that the tracking errors satisfy exponential convergence, and the prescribed performance constraints are guaranteed.*

Proof. Lyapunov function candidate is selected as:

$$\varphi_0 = \sum_{i=1}^{3}\varphi_i, \tag{51}$$

where φ_i are defined as:

$$\begin{aligned}\varphi_1 &= \frac{1}{2}s_1^2 + \frac{1}{2}y_2^2 + \frac{1}{2\alpha_1}\tilde{w}_1^2 + \frac{1}{2\beta_1}\tilde{R}_1^2,\\ \varphi_2 &= \frac{1}{2}s_2^2 + \frac{1}{2}y_3^2,\\ \varphi_3 &= \frac{1}{2}s_3^2 + \frac{\rho_1}{2k_7}\tilde{\eta}_1^2 + \frac{1}{2\alpha_3}\tilde{w}_3^2 + \frac{1}{2\beta_3}\tilde{R}_3^2.\end{aligned} \tag{52}$$

The differential of y_i, $i = 2, 3$, can be expressed as:

$$\begin{aligned}\dot{y}_i &= \dot{x}_{id} - \dot{x}_{ic} = -\frac{y_i}{\varepsilon_i} + B_i(\cdot),\\ B_i(\cdot) &= -\dot{x}_{ic}.\end{aligned} \tag{53}$$

It is worthy to point that there must exist constants $o_i > 0$, $i = 2, 3$, satisfying the inequality [32]:

$$|B_i(\cdot)| \le o_i, \tag{54}$$

in which o_1 are unknown positive constants.

Therefore, the time derivative of φ_i can be developed as:

$$\begin{aligned}\dot{\varphi}_1 &= s_1[m_1(f_1 + \mathrm{g}_1 x_2 - \dot{x}_{1d}) + n_1] + y_2\dot{y}_2 - \frac{1}{\alpha_1}\tilde{w}_1\dot{\widehat{w}}_1 - \frac{1}{\beta_1}\tilde{R}_1\dot{\widehat{R}}_1\\ &= s_1\left[m_1 f_1 + m_1\mathrm{g}_1 x_{e2} + m_1\mathrm{g}_1 y_2 - \widehat{w}_1 h_1 \tanh\left(\frac{s_1}{\mu_1}\right)\right.\\ &\quad - \widehat{R}_1 \tanh\left(\frac{s_1}{\mu_2}\right) + m_1\dot{x}_{1d} - m_1 g_1 x_{e2} - k_1 s_1 - k_2 \tanh(s_1)\\ &\quad \left.-n_1 - m_1\dot{x}_{1d} + n_1\right] + y_2\dot{y}_2 - \frac{1}{\alpha_1}\tilde{w}_1\dot{\widehat{w}}_1 - \frac{1}{\beta_1}\tilde{R}_1\dot{\widehat{R}}_1\\ &\le |s_1|(w_1 h_1 + R_1) + |m_1|\bar{\mathrm{g}}_1\left(\frac{s_1^2 + y_2^2}{2}\right) - \widehat{w}_1 h_1|s_1| + \mu_1\widehat{w}_1 h_1\kappa\\ &\quad - \widehat{R}_1|s_1| + \mu_2\widehat{R}_1\kappa - k_1 {s_1}^2 - k_2|s_1| + k_2\kappa - \left(\frac{1}{\varepsilon_2} - \frac{1}{2}\right)y_2^2\\ &\quad + \frac{o_2^2}{2} - \frac{1}{\alpha_1}\tilde{w}_1\alpha_1\left[|s_1|h_1 \tanh\left(\frac{|s_1|}{\mu_1}\right) - c_1\widehat{w}_1\right] - \frac{1}{\beta_1}\tilde{R}_1\beta_1\\ &\quad \cdot\left[|s_1| \tanh\left(\frac{|s_1|}{\mu_2}\right) - c_2\widehat{R}_1\right],\end{aligned}$$

$$\leq -\left(k_1 - \frac{|m_1|\bar{g}_1}{2}\right){s_1}^2 - \left(\frac{1}{\varepsilon_2} - \frac{|m_1|\bar{g}_1}{2} - \frac{1}{2}\right)y_2^2 + \frac{o_2^2}{2} + c_1\tilde{w}_1\widehat{w}_1 + c_2\tilde{R}_1\widehat{R}_1 + \mu_1 w_1 h_1\kappa + \mu_2 R_1\kappa + k_2\kappa \leq -\left(k_1 - \frac{|m_1|\bar{g}_1}{2}\right){s_1}^2 - \left(\frac{1}{\varepsilon_2} - \frac{|m_1|\bar{g}_1}{2} - \frac{1}{2}\right)y_2^2 - \frac{c_1}{2}\tilde{w}^2{}_1 - \frac{c_2}{2}\tilde{R}_1^2 + \frac{c_1}{2}w_1^2 + \frac{c_2}{2}R_1^2 + \frac{o_2^2}{2} + \mu_1 w_1 h_1\kappa + \mu_2 R_1\kappa + k_2\kappa = -\theta_1\varphi_1 + \zeta_1, \tag{55}$$

where $\theta_1 = \min\,(2k_1 - |m_1|\bar{g}_1, (2/\varepsilon_2) - |m_1|\bar{g}_1 - 1, \alpha_1 c_1, \beta_1 c_2)$, $\zeta_1 = (c_1/2)w_1^2 + (c_2/2)R_1^2 + (o_2^2/2) + \mu_1 w_1 h_1 \kappa + \mu_2 R_1\kappa + k_2\kappa$.

With the application of Equations (41)–(44), the time derivative of φ_2 can be expressed as:

$$\begin{aligned}\dot{\varphi}_2 &= s_2[m_2(x_3 - \dot{x}_{2d}) + n_2] + y_3\dot{y}_3 = s_2[m_2(x_{e3} + y_3 + x_{3c} - \dot{x}_{2d}) + n_2] + y_3\dot{y}_3 \\ &= s_2[m_2x_{e3} + m_2y_3 + m_2\dot{x}_{2d} - k_3s_2 - k_4\tanh(s_2) - m_2x_{e3} - n_2 - m_2\dot{x}_{2d} + n_2] + y_3\dot{y}_3 \leq s_2[m_2y_3 - k_3s_2 - k_4\tanh(s_2)] \\ &\quad - \frac{y_3^2}{\varepsilon_3} + |y_3||o_3| \leq |m_2|s_2y_3 - k_3{s_2}^2 - k_4|s_2| + k_4\kappa - \frac{y_3^2}{\varepsilon_3} + |y_3||o_3| \\ &\leq -\left(k_3 - \frac{|m_2|}{2}\right){s_2}^2 - \left(\frac{1}{\varepsilon_3} - \frac{|m_2|}{2} - \frac{1}{2}\right)y_3^2 + \frac{o_3^2}{2} + k_4\kappa \\ &= -\theta_2\varphi_2 + \zeta_2,\end{aligned} \tag{56}$$

where $\theta_2 = \min\,(2k_3 - |m_2|, (2/\varepsilon_3) - |m_2| - 1,)$, $\zeta_2 = (o_3^2/2) + k_4\kappa$.

With the substitution of Equations (47)–(50), the time derivative of φ_3 is written as:

$$\begin{aligned}\dot{\varphi}_3 &= s_3[m_3(f_3 + g_3(\rho_1 u_{c1} + d_1(\mathrm{t}) + \Delta_1) - \dot{x}_{3d}) + n_3] - \frac{\rho_1}{k_7}\tilde{\eta}_1\dot{\hat{\eta}}_1 - \frac{1}{\alpha_3}\tilde{w}_3\dot{\hat{w}}_3 - \frac{1}{\beta_3}\tilde{R}_3\dot{\hat{R}}_3 \leq |s_3|(w_3h_3 + r_3) \\ &\quad + m_3s_3[(1-\rho_1)u_{\mathrm{nom}1} - u_{\mathrm{nom}1} - \rho_1 u_{n1} - \dot{x}_{3d}] + n_3s_3 + |m_3|\,\bar{g}_3\lambda_1|s_3| - \frac{\rho_1}{k_7}\tilde{\eta}_1 k_7\left[|u_{\mathrm{nom}1}||s_3|\tanh\left(\frac{|u_{\mathrm{nom}1}||s_3|}{\mu_5}\right) - k_8\widehat{\eta}_1\right] \\ &\quad - \frac{1}{\alpha_3}\tilde{w}_3\dot{\hat{w}}_3 - \frac{1}{\beta_3}\tilde{R}_3\dot{\hat{R}}_3 \leq |s_3|\tilde{w}_3h_3 + |s_3|\tilde{R}_3 - k_5s_3^2 - k_6|s_3| + |m_3||s_3|(1-\rho_1)|u_{\mathrm{nom}1}| - \rho_1\kappa\widehat{\eta}_1|u_{\mathrm{nom}1}||s_3| + \kappa(\mu_3\widehat{w}_3h_3 \\ &\quad + \mu_4\widehat{R}_3 + k_6 + \mu_5\rho_1\eta_1) - \rho_1\kappa\tilde{\eta}_1|u_{\mathrm{nom}1}||s_3| + \rho_1k_8\tilde{\eta}_1\widehat{\eta}_1 - \frac{1}{\alpha_3}\tilde{w}_3\dot{\hat{w}}_3 - \frac{1}{\beta_3}\tilde{R}_3\dot{\hat{R}}_3.\end{aligned} \tag{57}$$

By utilizing Equations (51) and (52), the above inequality can be rewritten as:

$$\begin{aligned}\dot{\varphi}_3 &\leq |s_3|\tilde{w}_3h_3 + |s_3|\tilde{R}_3 - k_5s_3^2 - k_6|s_3| + |m_3||s_3|(1-\rho_1)|u_{\mathrm{nom}1}| - \rho_1\kappa\widehat{\eta}_1|u_{\mathrm{nom}1}||s_3| + \kappa(\mu_3\widehat{w}_3h_3 + \mu_4\widehat{R}_3 + k_6 + \mu_5\rho_1\eta_1) \\ &\quad - \rho_1\kappa\tilde{\eta}_1|u_{\mathrm{nom}1}||s_3| + \rho_1k_8\tilde{\eta}_1\widehat{\eta}_1 - \frac{1}{\alpha_3}\tilde{w}_3\alpha_3 \cdot \left[|s_3|h_3\tanh\left(\frac{|s_3|}{\mu_3}\right) - c_5\widehat{w}_3\right], \\ &\quad - \frac{1}{\beta_3}\tilde{R}_3\beta_3\left[|s_3|\tanh\left(\frac{|s_3|}{\mu_4}\right) - c_6\widehat{R}_3\right] \leq -k_5s_3^2 + \rho_1k_8\tilde{\eta}_1\widehat{\eta}_1 + c_5\tilde{w}_3\widehat{w}_3 + c_6\tilde{R}_3\widehat{R}_3 + \kappa(\mu_3w_3h_3 + \mu_4R_3 + k_6 + \mu_5\rho_1\eta_1) \\ &\leq -k_5s_3^2 - \frac{\rho_1k_8}{2}\tilde{\eta}_1^2 - \frac{c_5}{2}\tilde{w}_3^2 - \frac{c_6}{2}\tilde{R}_3^2 + \frac{\rho_1k_8}{2}\eta_1^2 + \frac{c_5}{2}w_3^2 + \frac{c_6}{2}R_3^2 + \kappa(\mu_3w_3h_3 + \mu_4R_3 + k_6 + \mu_5\rho_1\eta_1) = -\theta_3\varphi_3 + \zeta_3,\end{aligned} \tag{58}$$

Table 1: Initial values of states.

Item	Value	Unit
V	15060	ft/s
h	110000	ft
γ	0	rad
α	$1.6325\pi/180$	rad
q	0	rad/s

where $\theta_3 = \min\,(2k_5, k_7k_8, \alpha_3c_5, \beta_3c_6)$, $\zeta_3 = \kappa(\mu_3w_3h_3 + \mu_4R_3 + k_6 + \mu_5\rho_1\eta_1) + (\rho_1k_8/2)\eta_1^2 + (c_5/2)w_3^2 + (c_6/2)R_3^2$.

Consequently, the differential of φ_0 can be calculated as:

$$\begin{aligned}\dot{\varphi}_0 &\leq -\left(k_1 - \frac{|m_1|\bar{g}_1}{2}\right){s_1}^2 - \left(\frac{1}{\varepsilon_2} - \frac{|m_1|\bar{g}_1}{2} - \frac{1}{2}\right)y_2^2 - \frac{c_1}{2}\tilde{w}^2{}_1 - \frac{c_2}{2}\tilde{R}_1^2 - \left(k_3 - \frac{|m_2|}{2}\right){s_2}^2 - \left(\frac{1}{\varepsilon_3} - \frac{|m_2|}{2} - \frac{1}{2}\right)y_3^2 - k_5s_3^2 \\ &\quad - \frac{\rho_1k_8}{2}\tilde{\eta}_1^2 - \frac{c_5}{2}\tilde{w}_3^2 - \frac{c_6}{2}\tilde{R}_3^2 + \frac{c_1}{2}w_1^2 + \frac{c_2}{2}R_1^2 + \frac{o_2^2}{2} + \mu_1w_1h_1\kappa + \mu_2R_1\kappa + k_2\kappa + \frac{o_3^2}{2} + k_4\kappa + \frac{\rho_1k_8}{2}\eta_1^2 \\ &\quad + \frac{c_5}{2}w_3^2 + \frac{c_6}{2}R_3^2 + \kappa(\mu_3w_3h_3 + \mu_4R_3 + k_6 + \mu_5\rho_1\eta_1) \\ &\leq -\theta_0\varphi_0 + \zeta_0,\end{aligned} \tag{59}$$

with

$$\theta_0 = \min\left(2k_1 - |m_1|\bar{g}_1, \frac{2}{\varepsilon_2} - |m_1|\bar{g}_1 - 1, \alpha_1c_1, \beta_1c_2, 2k_3 - |m_2|\bar{g}_2, \frac{2}{\varepsilon_3} - |m_2|\bar{g}_2 - 1, 2k_5, k_7k_8, \alpha_3c_5, \beta_3c_6\right), \tag{60}$$

$$\zeta_0 = \frac{c_1}{2}w_1^2 + \frac{c_2}{2}R_1^2 + \frac{o_2^2}{2} + \mu_1w_1h_1\kappa + \mu_2R_1\kappa + k_2\kappa + \frac{o_3^2}{2} + k_4\kappa + \frac{\rho_1k_8}{2}\eta_1^2 + \frac{c_6}{2}R_3^2 + \frac{c_5}{2}w_3^2 + \kappa(\mu_3w_3h_3 + \mu_4R_3 + k_6 + \mu_5\rho_1\eta_1). \tag{61}$$

To conclude, s_1, s_2, and s_3 exponentially converge to a neighborhood around the origin, only if the designed parameters $k_1, k_2, k_3, k_4, k_5, k_6, k_7, k_8, \alpha_1, \alpha_3, \beta_1, \beta_3, c_1, c_2, c_3, c_4, c_5,$

Table 2: Values of control parameters.

Section	Parameters
PPC	$x_{ei} = (\bar{\lambda}_i - \underline{\lambda}_i)\exp(-\iota_i t) + \underline{\lambda}_i, i = 0, 1, 2, 3, 4, \bar{\lambda}_0 = 105, \underline{\lambda}_0 = 3,$ $\iota_0 = 0.2, \bar{\lambda}_1 = 0.05, \underline{\lambda}_1 = 0.04, \iota_1 = 0.3, \bar{\lambda}_2 = 0.1, \underline{\lambda}_2 = 0.035,$ $\iota_2 = 0.1, \bar{\lambda}_1 = 0.1, \underline{\lambda}_1 = 0.05, \iota_1 = 0.1, \bar{\lambda}_1 = 105, \underline{\lambda}_1 = 5, \iota_1 = 0.1$
Low-pass filter	$\varepsilon_2 = 10, \varepsilon_3 = 10$
Input of MLP-NN	Referring to [35]
Controller	$k_h = 10, k_{hh} = 1.5, k_1 = 0.8, k_2 = 0.2, \alpha_1 = 0.0001, c_1 = 2,$ $\beta_1 = 0.001, c_2 = 10, k_3 = 2.5, k_4 = 0.01, k_5 = 0.05, k_6 = 0.05,$ $k_7 = 0.05, k_8 = 30, \alpha_3 = 0.001, c_5 = 10, \beta_3 = 0.05, c_6 = 10,$ $k_9 = 3, k_{10} = 2, k_{11} = 0.005, k_{12} = 2, \alpha_4 = 0.05, c_7 = 2, \beta_4 = 0.01, c_8 = 2$

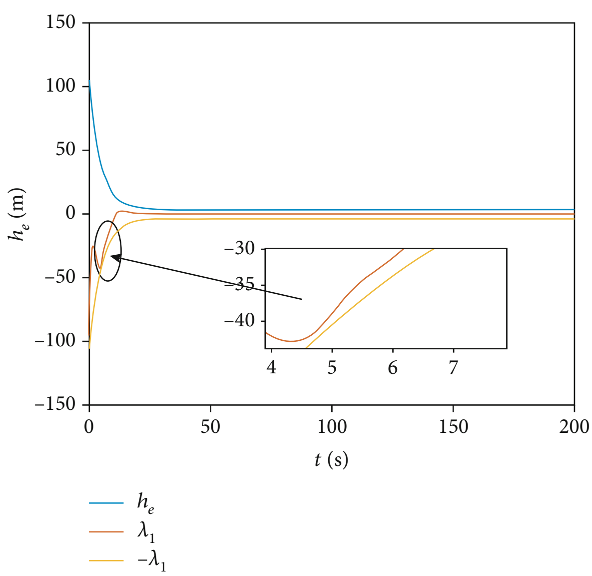

Figure 1: The altitude tracking error of HFV.

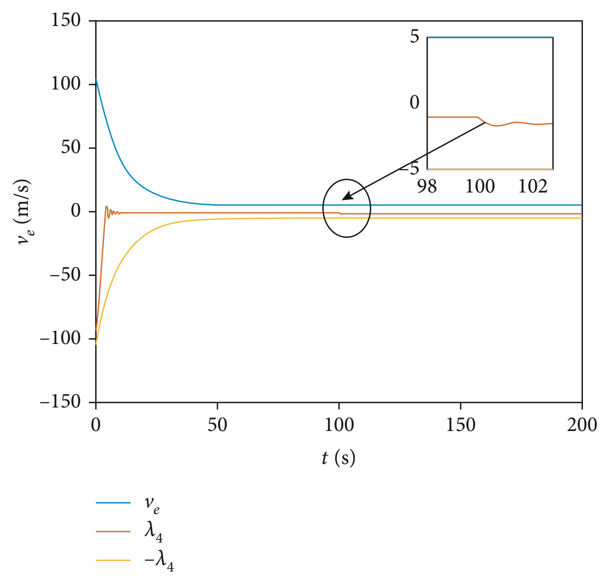

Figure 2: The velocity tracking error of HFV.

c_6, μ_1, μ_2, μ_3, μ_4, and μ_5 are chosen to satisfy $\theta_0 > 0$. According to the transformation Equation (26), the stabilization of tracking errors x_{ei} is guaranteed, while their trajectories always remain within the predefined region. The proof of Theorem 5 is completed.

4. Velocity Controller Design

The velocity tracking control subsystem for HFVs is established as:

$$\dot{V} = f_v + \rho_2 u_{c2} + d_2(\mathrm{t}) + \Delta_2. \tag{62}$$

The definition of velocity tracking error V_e and its time derivative are given as:

$$\begin{aligned} V_e &= V - V_d, \\ \dot{V}_e &= \dot{V} - \dot{V}_d = f_v + \rho_2 u_{c2} + d_2(t) + \Delta_2 - \dot{V}_d. \end{aligned} \tag{63}$$

The predesigned boundary of variable V_e is denoted as:

$$\underline{V}_e \le V_e \le \bar{V}_e. \tag{64}$$

The error transformation is redesigned as:

$$\begin{aligned} V_e &= \frac{\bar{V}_e + \underline{V}_e}{2}\tanh(s_4) + \frac{\bar{V}_e + \underline{V}_e}{2}, \\ s_4 &= \operatorname{atanh}\left(\frac{2V_e - \bar{V}_e - \underline{V}_e}{\bar{V}_e - \underline{V}_e}\right), \end{aligned} \tag{65}$$

where s_4 is the transformed velocity error. Obviously, it indicates that the transformed error increases monotonically with the original error.

Hence, there exist limits as:

$$\lim_{s_4 \to -\infty} V_e = \underline{V}_e, \lim_{s_4 \to +\infty} V_e = \bar{V}_e. \tag{66}$$

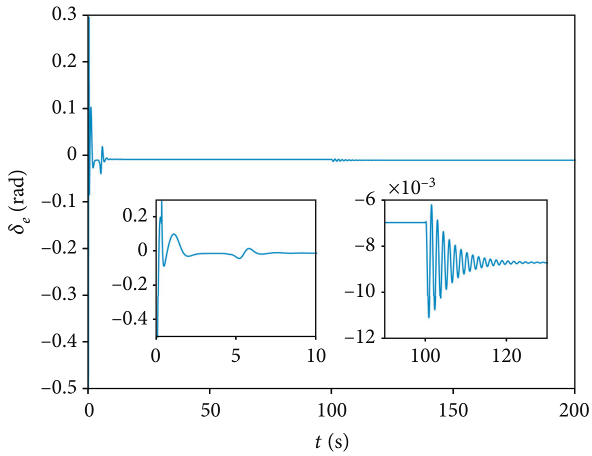

Figure 3: The input signal of altitude control subsystem.

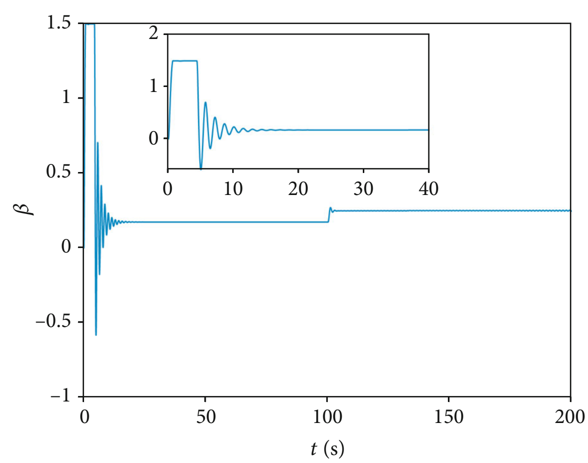

Figure 4: The input signal of velocity control subsystem.

Additionally, the time derivative of s_4 is derived as:

$$\begin{aligned}\dot{s}_4 &= m_4 \dot{V}_e + n_4 \\ &= m_4\left(f_v + \rho_2 u_{c2} + d_2(t) + \Delta_2 - \dot{V}_d\right) + n_4.\end{aligned} \tag{67}$$

Subsequently, the uncertain dynamic $m_4 f_v$ is approximated by adopting RBFNN, which can be expressed as:

$$m_4 f_v = \mathbf{W}_{v1}^{*T} \mathbf{H}_{v1}(\mathbf{x}) + r_v, 0 < |r_v| \le O_v, \tag{68}$$

$$\left\|\mathbf{W}_{v1}^{*T} \mathbf{H}_{v1}\right\| \le \left\|\mathbf{W}_{v1}^{*T}\right\| \left\|\mathbf{H}_{v1}\right\| \le w_v h_v, \tag{69}$$

where $h_v = \|\mathbf{H}_{v1}\|$ and $w_v \ge \|\mathbf{W}_{v1}^{*T}\|$.

The control input and adaptive laws are given as:

$$u_{c2} = -(u_{\text{nom2}} + u_{n2}), \tag{70}$$

$$\begin{aligned}u_{\text{nom2}} = \frac{1}{m_4}\Bigg[&\widehat{\omega}_v h_v \tanh\left(\frac{s_4}{\mu_6}\right) + \widehat{R}_4 \tanh\left(\frac{s_4}{\mu_7}\right) \\ &+ k_9 s_4 + k_{10} \tanh(s_4) + n_4\Bigg] - \dot{v}_d,\end{aligned} \tag{71}$$

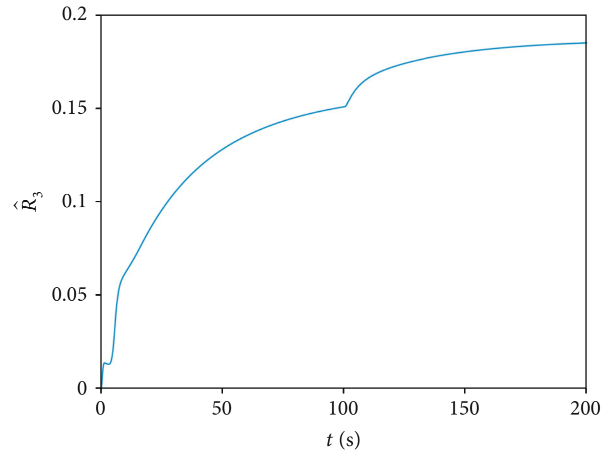

Figure 5: Estimation of R_3.

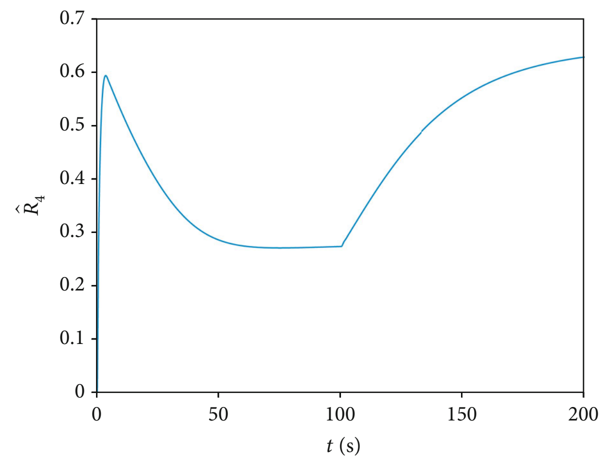

Figure 6: Estimation of R_4.

$$u_{n2} = \frac{1}{m_4} \widehat{\eta}_2 |u_{\text{nom2}}| \tanh\left(\frac{|u_{\text{nom2}}| s_4}{\mu_8}\right), \tag{72}$$

$$\dot{\widehat{\eta}}_2 = k_{11}\left[|u_{\text{nom2}}||s_4| \tanh\left(\frac{|u_{\text{nom2}}||s_4|}{\mu_8}\right) - k_{12}\widehat{\eta}_2\right], \tag{73}$$

$$\dot{\widehat{\omega}}_v = \alpha_4\left[h_v |s_4| \tanh\left(\frac{|s_4|}{\mu_6}\right) - c_7 \widehat{\omega}_v\right], \tag{74}$$

$$\dot{\widehat{R}}_4 = \beta_4\left[|s_4| \tanh\left(\frac{|s_4|}{\mu_7}\right) - c_8 \widehat{R}_4\right], \tag{75}$$

where $\eta_2 = ((1-\rho_2)m_4)/\rho_2$ and $R_4 = m_4\lambda_2 + O_v$; $\widehat{\eta}_2$, $\widehat{\omega}_v$, and $\widehat{R}_4$ are the estimate values of η_2, w_v, and R_4, respectively; and $k_9, k_{10}, k_{11}, k_{12}, \alpha_4, \beta_4, c_7, c_8, \mu_6, \mu_7$, and μ_8 are all positive parameters.

Theorem 6. *Noting the velocity dynamic (61) of HFV and considering the fault tolerant controller Equations (69)–(71), exponential convergence and prescribed performance constraints will be ensured for the tracking error.*

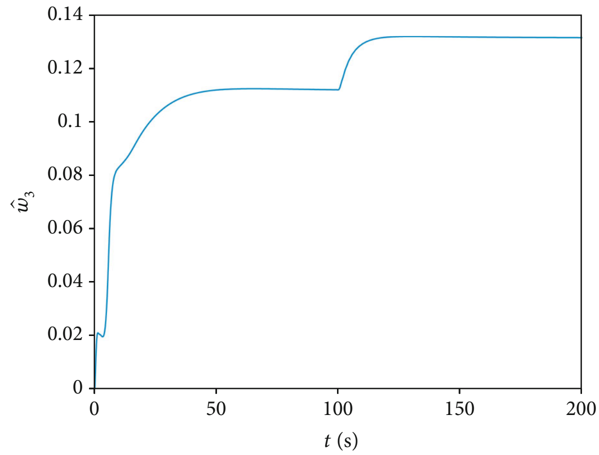

Figure 7: Estimation of w_3.

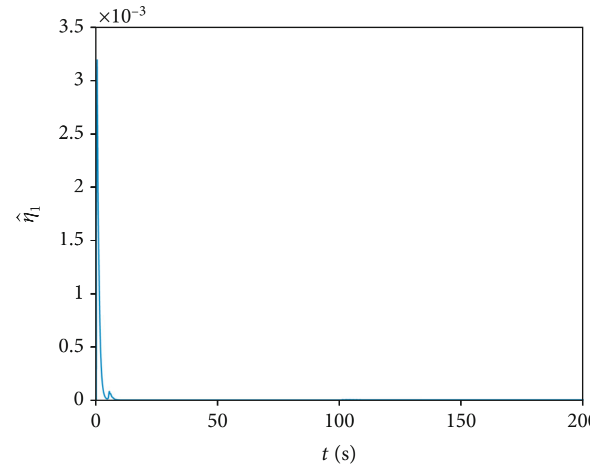

Figure 9: Estimation of η_1.

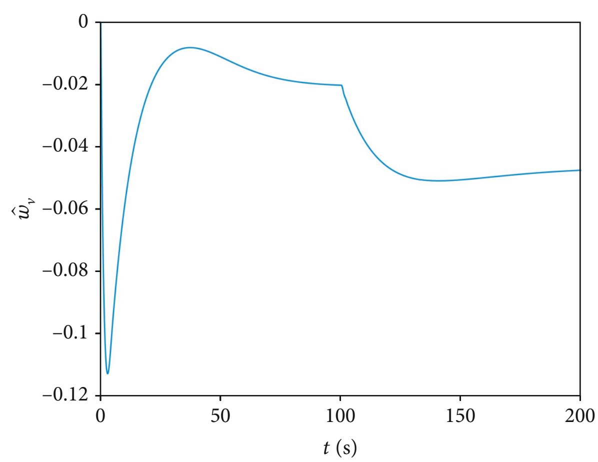

Figure 8: Estimation of w_v.

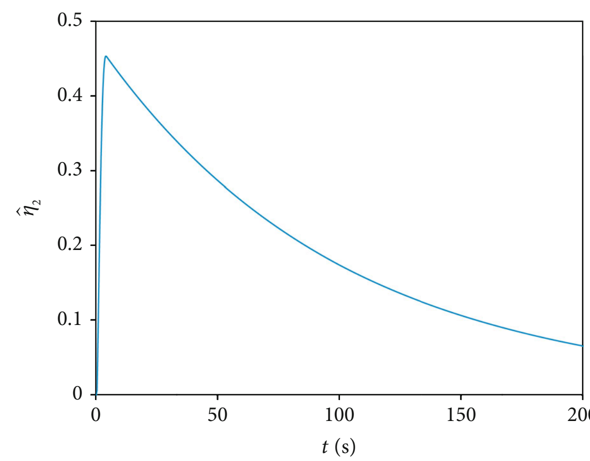

Figure 10: Estimation of η_2.

Proof. To illustrate the convergence of velocity tracking error, the Lyapunov function is selected as:

$$\varphi_4 = \frac{1}{2}s_4^2 + \frac{\rho_2}{2k_{11}}\tilde{\eta}_2^2 + \frac{1}{2\alpha_4}\tilde{w}_v^2 + \frac{1}{2\beta_4}\tilde{R}_4^2. \tag{76}$$

With the substitution of Equations (69)–(71), the time derivative of φ_4 is derived as:

$$\begin{aligned}\dot{\varphi}_4 &= s_4 m_4\left[f_v + \rho_2 u_c + d_2(t) + \Delta_2 - \dot{v}_d\right] + n_4 s_4 - \frac{\rho_2}{k_{11}}\tilde{\eta}_2\dot{\hat{\eta}}_2 \\ &\quad - \frac{1}{\alpha_4}\tilde{w}_v\dot{\hat{w}}_v - \frac{1}{\beta_4}\tilde{R}_4\dot{\hat{R}}_4 \le |s_4|(w_v h_v + R_v) + m_4 s_4 \\ &\quad \cdot \left[(1-\rho_2)u_{\text{nom2}} - u_{\text{nom2}} - \rho_2 u_{n2} - \dot{v}_d\right] + n_4 s_4 \\ &\quad - \frac{\rho_2}{k_{11}}\tilde{\eta}_2\dot{\hat{\eta}}_2 - \frac{1}{\alpha_4}\tilde{w}_v\dot{\hat{w}}_v - \frac{1}{\beta_4}\tilde{R}_4\dot{\hat{R}}_4 \le |s_4|\tilde{w}_v h_v + |s_4|\tilde{R}_4 \\ &\quad - k_9 s_4^2 - k_{10}|s_4| + |m_4||s_4|(1-\rho_2)|u_{\text{nom2}}| - \rho_2|u_{\text{nom2}}||\hat{\eta}_2||s_4| \\ &\quad + \kappa(\mu_6\hat{w}_v h_v + \mu_7\hat{R}_4 + k_{10} + \mu_8\rho_2\eta_2) - \rho_2|u_{\text{nom2}}||\tilde{\eta}_2||s_4| \\ &\quad + \rho_2 k_{12}\tilde{\eta}_2\hat{\eta}_2 - \frac{1}{\alpha_4}\tilde{w}_v\dot{\hat{w}}_v - \frac{1}{\beta_4}\tilde{R}_4\dot{\hat{R}}_4.\end{aligned} \tag{77}$$

Taking Equations (71)–(73) into account, Equation (77) can be further expressed as:

$$\begin{aligned}\dot{\varphi}_4 &\le |s_4|\tilde{w}_v h_v + |s_4|\tilde{R}_4 - k_9 s_4^2 - k_{10}|s_4| + |m_4||s_4|(1-\rho_2)|u_{\text{nom2}}| \\ &\quad - \rho_2|u_{\text{nom2}}||\hat{\eta}_2||s_4| + \kappa(\mu_6\hat{w}_v h_v + \mu_7\hat{R}_4 + k_{10} + \mu_8\rho_2\eta_2) \\ &\quad - \rho_2|u_{\text{nom2}}||\tilde{\eta}_2||s_4| + \rho_2 k_{12}\tilde{\eta}_2\hat{\eta}_2 - \frac{1}{\alpha_4}\tilde{w}_v\alpha_4 \\ &\quad \cdot \left[h_v|s_4| \tanh\left(\frac{|s_4|}{\mu_6}\right) - c_7\hat{w}_v\right] - \frac{1}{\beta_4}\tilde{R}_4\beta_4 \\ &\quad \cdot \left[|s_4| \tanh\left(\frac{|s_4|}{\mu_7}\right) - c_8\hat{R}_4\right] \le -k_9 s_4^2 + \rho_2 k_{12}\tilde{\eta}_2\hat{\eta}_2 \\ &\quad + c_7\tilde{w}_v\hat{w}_v + c_8\tilde{R}_4\hat{R}_4 + \kappa(\mu_6 w_v h_v + \mu_7 R_4 + k_{10} + \mu_8\rho_2\eta_2) \\ &\le -k_9 s_4^2 - \frac{\rho_2 k_{12}}{2}\tilde{\eta}_2^2 - \frac{c_7}{2}\tilde{w}^2{}_v - \frac{c_8}{2}\tilde{R}_4^2 + \frac{\rho_2 k_{12}}{2}\eta_2^2 + \frac{c_7}{2}w_v^2 \\ &\quad + \frac{c_8}{2}R_4^2 + \kappa(\mu_6 w_v h_v + \mu_7 R_4 + k_{10} + \mu_8\rho_2\eta_2) = -\theta_4\varphi_4 + \zeta_4,\end{aligned} \tag{78}$$

where $\theta_4 = \min\left(2k_9, k_{11}k_{12}, \alpha_4 c_7, \beta_4 c_8\right)$ and $\zeta_4 = (\rho_2 k_{12}/2)\eta_2^2 + (c_7/2)w_v^2 + \kappa(\mu_6 w_v h_v + \mu_7 R_4 + k_{10} + \mu_8\rho_2\eta_2) + (c_8/2)R_4^2$.

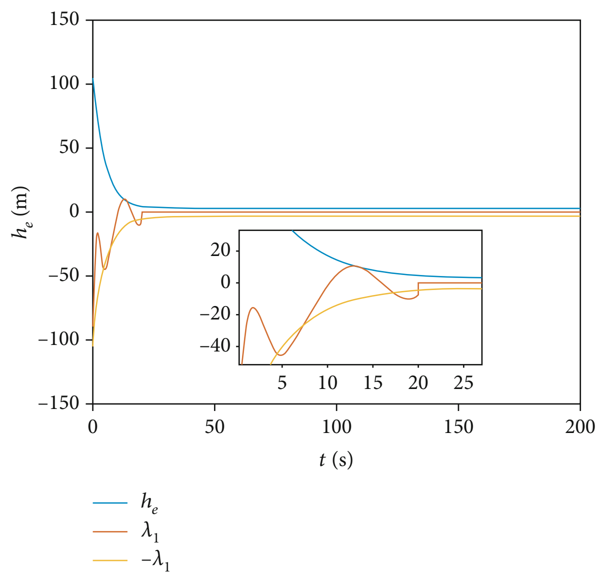

Figure 11: The tracking error of altitude without PPC.

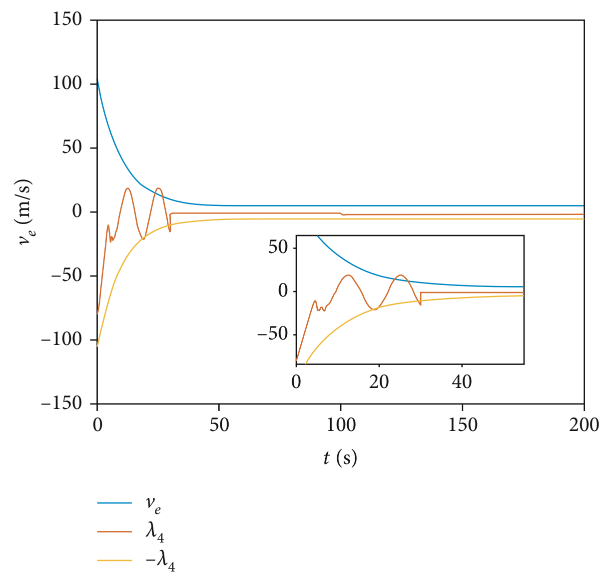

Figure 12: The tracking error of velocity without PPC.

Therefore, it can be concluded that s_4 is asymptotically stable, and the velocity tracking error V_e completes convergence within the prespecified range. Theorem 6 is validated sufficiently.

5. Simulation

To illustrate the specific performances of the proposed controller, a numerical simulation is executed based on the longitudinal dynamics (1)–(17) of HFV. By giving the initial states and reference trajectories, the tracking control objective will be achieved with predefined performance constraints. The initial values of states are provided in Table 1, and the control parameters are shown in Table 2.

Meanwhile, the desired trajectories, environmental disturbances, and actuator effectiveness parameters are defined as:

$$\begin{aligned} &V_d = 15160\text{ft/}s, h_d = 110100\text{ft}, \\ &d_1 = 0.01 \times \sin(0.05\text{t}), d_2 = 0.01 \times \cos(0.05t), \\ &\rho_1 = \begin{cases} 1, & t < 100s \\ 0.7, & t \geq 100s \end{cases}, \Delta_1 = 0.001 \times \sin(0.05t), \\ &\rho_2 = \begin{cases} 1, & t < 100s \\ 0.8, & t \geq 100s \end{cases}, \Delta_2 = 0.001 \times \cos(0.05t). \end{aligned} \tag{79}$$

Consequently, the main results are exhibited in Figures 1–10. Firstly, the curves of tracking errors are shown in Figures 1 and 2. It follows from these two pictures that the altitude tracking error and velocity tracking error are stabilized into a tiny neighborhood around origin within 30 s and 50 s, respectively. Obviously, not only the transient performance constraint is guaranteed but also the steady-state errors are maintained within ranges of 5 m and 5 m/s, which means undoubtedly a very high accuracy for hypersonic flight. What is subsequently given in Figures 3 and 4 is the curves of control inputs. In particular, even if there is an unknown actuator failure occurring at 100 s, the control signal is capable of returning to a constant within an extremely short time. Figures 5 and 6 show the curves of adaptive estimates $\hat{R}_3$ and $\hat{R}_4$, which always remain bounded under the designed algorithm. The estimations about weight matrixes of RBFNNs are provided in Figures 7 and 8, and the adaptive learning parameters for actuator failure are settled in Figures 9 and 10. As is shown in figures, all the estimations finally converge to constants. Thus, the proposed controller is capable of tracking the desired trajectory in case of actuator faults.

For better illustration of the merits PPC, simulation results without performance constraints are presented in Figures 11 and 12. Observing the tracking errors of altitude and velocity, one can conclude that the performance constraints will be violated before the system's stabilization. From this aspect, it deduces that the PPC control strategies are necessary for hypersonic vehicles' tracking control.

6. Conclusion

This study concentrates on the robust prescribed performance tracking control for HFV in the presence of system uncertainties and unknown actuator faults. On the basis of longitudinal model of HFV, an antidisturbance neural adaptive control strategy is constructed, in which MLP algorithm is employed to approximate the unavailable dynamics with a reduced computational burden. In addition, the multiplicative and additive failures of actuator are taken into account simultaneously. Finally, the stability and effectiveness of proposed controller are elaborated by rigorous theoretical analysis. The results of simulation example further indicate that the altitude and velocity tracking errors satisfy the prescribed performance constraints.

Data Availability

The data used to support the findings of this study are available from the corresponding author upon request.

Conflicts of Interest

The authors declare that they have no conflicts of interest.

References

[1] H. Xu, M. D. Mirmirani, and P. A. Ioannou, "Adaptive sliding mode control design for a hypersonic flight vehicle," *Journal of Guidance, Control, and Dynamics*, vol. 27, no. 5, pp. 829–838, 2004.

[2] J. Wang, Q. Zong, R. Su, and B. Tian, "Continuous high order sliding mode controller design for a flexible air- breathing hypersonic vehicle," *ISA Transactions*, vol. 53, no. 3, pp. 690–698, 2014.

[3] J. Guo, S. Yalu, X. Wang, and J. Zhou, "Iterative-learning-based sliding mode control design for hypersonic vehicles with wind effects," *Transactions of the Institute of Measurement and Control*, vol. 42, no. 10, pp. 1769–1781, 2020.

[4] Q. Ma, J. Guo, and J. Zhou, "A finite-time sliding mode control for hypersonic vehicle," *Transactions of the Institute of Measurement and Control*, vol. 41, no. 15, pp. 4339–4350, 2019.

[5] Z. Shen, Q. Wang, G. Yang, and M. Zhang, "Anti-disturbance backstepping control for air-breathing hypersonic vehicles based on extended state observer," *ISA Transactions*, vol. 92, 2019.

[6] F. Liao, H. Ji, and B. Yu, "Controller design for hypersonic vehicle via backstepping and ISS," in *Proceedings of the 31st Chinese Control Conference*, pp. 1030–1035, Hefei, China, 2012.

[7] Y. Huang, R. Qi, B. Jiang, and G. Tao, "Adaptive failure compensation design for hypersonic vehicle based on dynamic surface backstepping control," in *Proceedings of the 31st Chinese Control Conference*, pp. 5305–5310, Hefei, China, 2012.

[8] L. H. Yan, M. Zhu, and L. Jing, "Robust backstepping control with prescribed performance for inner-loop longitudinal system of hypersonic vehicles under input constraint," *Journal of Interdisciplinary Mathematics*, vol. 22, no. 6, pp. 873–888, 2019.

[9] Z. Shen, Q. Wang, and C. Dong, "A novel adaptive dynamic surface control scheme of hypersonic flight vehicles with thrust and actuator constraints," *Transactions of the Institute of Measurement and Control*, vol. 40, no. 4, pp. 1362–1374, 2018.

[10] L. Zhou and L. Yin, "Dynamic surface control based on neural network for an air-breathing hypersonic vehicle," *Optimal Control Applications and Methods*, vol. 36, no. 6, pp. 774–793, 2015.

[11] B. Xu, Q. Zhang, and Y. Pan, "Neural network based dynamic surface control of hypersonic flight dynamics using small-gain theorem," *Neurocomputing*, vol. 173, pp. 690–699, 2016.

[12] J. Chen, Y. Lin, and C. P. Pan, "One near space hypersonic aircraft neural networks dynamic surface backstepping control design," *Applied Mechanics and Materials*, vol. 2963, pp. 1068–1071, 2014.

[13] C. Zhu, B. Huang, B. Zhou, Y. Su, and E. Zhang, "Adaptive model-parameter-free fault-tolerant trajectory tracking control for autonomous underwater vehicles," *ISA transactions*, 2021.

[14] B. Huang, A. Li, Y. Guo, and C. Q. Wang, "Fixed-time attitude tracking control for spacecraft without unwinding," *Acta Astronautica*, vol. 151, pp. 818–827, 2018.

[15] B. Huang, A. Li, Y. Guo, and C. Q. Wang, "Rotation matrix based finite-time attitude synchronization control for spacecraft with external disturbances," *ISA Transactions*, vol. 85, pp. 141–150, 2019.

[16] B. Huang, S. Zhang, Y. He, B. Wang, and Z. Deng, "Finite-time anti-saturation control for Euler-Lagrange systems with actuator failures," *ISA transactions*, 2020.

[17] R. S. Xia, M. Chen, Q. X. Wu, and Y. H. Wang, "Neural network based integral sliding mode optimal flight control of near space hypersonic vehicle," *Neurocomputing*, vol. 379, pp. 41–52, 2020.

[18] B. Huang, B. Zhou, S. Zhang, and C. Zhu, "Adaptive prescribed performance tracking control for underactuated autonomous underwater vehicles with input quantization," *Ocean Engineering*, vol. 221, p. 108549, 2021.

[19] X. Shao, X. Yue, and J. Li, "Event-triggered robust control for quadrotors with preassigned time performance constraints," *Applied Mathematics and Computation*, vol. 392, p. 125667, 2021.

[20] X. Shao, Y. Shi, and W. Zhang, "Fault-tolerant quantized control for flexible air-breathing hypersonic vehicles with appointed-time tracking performances," *IEEE Transactions on Aerospace and Electronic Systems*, 2020.

[21] Y. Wang and J. Hu, "Improved prescribed performance control for air-breathing hypersonic vehicles with unknown deadzone input nonlinearity," *ISA Transactions*, vol. 79, pp. 95–107, 2018.

[22] B. Xiangwei, "Guaranteeing prescribed performance for air-breathing hypersonic vehicles via an adaptive non-affine tracking controller," *Acta Astronautica*, vol. 151, pp. 368–379, 2018.

[23] X. Shao, Y. Shi, W. Zhang, and H. Cao, "Neurodynamic approximation-based quantized control with improved transient performances for MEMS gyroscopes: theory and experimental results," *IEEE Transactions on Industrial Electronics*, 2020.

[24] X. Shao, Z. Cao, and H. Si, "Neurodynamic formation maneuvering control with modified prescribed performances for networked uncertain quadrotors," *IEEE Systems Journal*, pp. 1–12, 2020.

[25] J. G. Sun, S. M. Song, and W. G. Q. Peng-Li, "Adaptive anti-saturation fault-tolerant control of hypersonic vehicle with actuator faults," *Proceedings of the iInstitution of mMechanical eEngineers, Part G: Journal of Aerospace Engineering*, vol. 233, no. 6, pp. 2066–2083, 2019.

[26] Z. Cheng, F. Chen, and J. Niu, "Quasi-continuous high-order sliding mode control-based fault-tolerant control for hypersonic flight vehicle via neural network observer," *Proceedings of the Institution of Mechanical Engineers, Part G: Journal of Aerospace Engineering*, vol. 233, no. 5, pp. 1784–1800, 2019.

[27] S. Zhao and X. Li, "Prescribed performance fault tolerant control for hypersonic flight vehicles with actuator failures," *IEEE Access*, vol. 7, pp. 100187–100204, 2019.

[28] Q. Shen, D. Wang, S. Zhu, and K. Poh, "Finite-time fault-tolerant attitude stabilization for spacecraft with actuator saturation," *IEEE Transactions on Aerospace and Electronic Systems*, vol. 51, no. 3, pp. 2390–2405, 2015.

[29] J. T. Parker, A. Serrani, S. Yurkovich, M. A. Bolender, and D. B. Doman, "Control-oriented modeling of an air-breathing hypersonic vehicle," *Journal of Guidance, Control, and Dynamics*, vol. 30, no. 3, pp. 856–869, 2007.

[30] H. Sun, S. Li, and C. Sun, "Robust adaptive integral-sliding-mode fault-tolerant control for airbreathing hypersonic vehicles," *Proceedings of the Institution of Mechanical Engineers, Part I: Journal of Systems and Control Engineering*, vol. 226, pp. 1344–1355, 2012.

[31] B. Xu, D. Gao, and S. Wang, "Adaptive neural control based on HGO for hypersonic flight vehicles," *Science China Information Sciences*, vol. 54, no. 3, pp. 511–520, 2011.

[32] F. Chen, Z. Wang, G. Tao, and B. Jiang, "Robust adaptive fault-tolerant control for hypersonic flight vehicles with multiple faults," *Journal of Aerospace Engineering*, vol. 28, no. 4, p. 4014111, 2014.

[33] C. Wei, J. Luo, C. Ma, H. Dai, and J. Yuan, "Event-triggered neuroadaptive control for postcapture spacecraft with ultralow-frequency actuator updates," *Neurocomputing*, vol. 315, pp. 310–321, 2018.

[34] B. Huang, A. Li, and B. Xu, "Adaptive fault tolerant control for hypersonic vehicle with external disturbance," *International Journal of Advanced Robotic Systems*, vol. 14, no. 1, p. 1729881416687136, 2017.

[35] Z. Wu, J. Lu, J. Shi, Q. Zhou, and X. Qu, "Tracking error constrained robust adaptive neural prescribed performance control for flexible hypersonic flight vehicle," *International Journal of Advanced Robotic Systems*, vol. 14, no. 1, p. 1729881416682704, 2017.